Image Cover Sheet

CLASSIFICATION	SYSTEM NUMBER
UNCLASSIFIED	153071

TITLE

DESIGN CONSIDERATIONS FOR AS SUBOPTIMAL FILTER

System Number:

Patron Number:

Requester:

Notes: Paper #13 of Multipart document Sysnum #153027

DSIS Use only:

Deliver to: DK

Design Considerations for a Suboptimal Kalman Filter

D.J.DiFilippo
Defence Research Establishment Ottawa
Ottawa, Canada
K1A 0Z4

1. INTRODUCTION

In designing a suboptimal Kalman filter, the designer must decide how to simplify the system error model without causing the filter estimation errors to increase to unacceptable levels. Deletion of certain error states and decoupling of error state dynamics are the two principal model simplifications that are commonly used in suboptimal filter design. For the most part, the decisions as to which error states can be deleted or decoupled are based on the designer's understanding of the physics of the particular system. Consequently, the details of a suboptimal design are usually unique to the specific application.

In this paper, the process of designing a suboptimal Kalman filter is illustrated for the case of an airborne *t*ransfer-*o*f-*a*lignment (TOA) system used for *s*ynthetic *a*perture *r*adar (SAR) motion compensation. In this application, the filter must continuously transfer the alignment of an onboard Doppler-damped master *i*nertial *n*avigation *s*ystem (INS) to a strapdown navigator that processes information from a less accurate *i*nertial *m*easurement *u*nit (IMU) mounted on the radar antenna. The IMU is used to measure spurious antenna motion during the SAR imaging interval, so that compensating phase corrections can be computed and applied to the radar returns, thereby preventing image degradation that would otherwise result from such motions. The principles of SAR are described in many references, for instance [1], [2].

The primary function of the TOA Kalman filter in a SAR motion compensation system is to control strapdown navigator attitude errors, and to a lesser degree, velocity and heading errors. Unlike a classical navigation application, absolute positional accuracy is not important. The motion compensation requirements for SAR imaging are discussed in some detail in [3]. This TOA application is particularly appropriate as a vehicle for discussing suboptimal filter design, because the system contains features that can be exploited to allow both deletion and decoupling of error states.

In Section 2, a high-level background description of a SAR motion compensation system that incorporates a TOA Kalman filter is given. The optimal TOA filter design is presented in Section 3 with some simulation results to indicate potential filter performance. In Section 4, the suboptimal Kalman filter configuration is derived. Simulation results are also shown in this section to allow comparison between suboptimal and optimal filter performances. Conclusions are contained in Section 5.

Throughout this paper, it is assumed that the reader is familiar with basic Kalman filter theory. If not, a treatment of this subject can be found in [4], [5] or [6].

2. SAR MOTION COMPENSATION SYSTEM DESCRIPTION

2.1 Sensors

A functional block diagram of a SAR *m*otion *c*ompensation *s*ystem (SARMCS) that utilizes a TOA Kalman filter is shown in Figure 1.

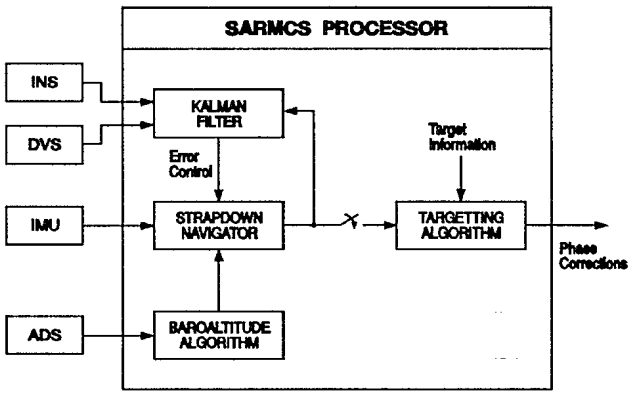

Figure 1. Functional Block Diagram of a SARMCS

The principal motion compensation sensor is a small *i*nertial *m*easurement *u*nit (IMU) mounted directly on the antenna structure. It provides raw measurements of the angular rates and linear accelerations of the antenna in the standard form of angular and velocity increments. The antenna structure is assumed to be physically stabilized in roll and pitch. Consequently, the strapdown IMU is exposed to only residual angular motion about the aircraft's roll and pitch axes resulting from imperfect antenna stabilization, while it is fully exposed to angular motion caused by aircraft heading changes. It is assumed that the IMU contains two dry tuned-rotor gyroscopes and three accelerometers with the specifications shown in Table 1.

The onboard master *i*nertial *n*avigation *s*ystem (INS) is remotely located from the IMU. It is assumed to be a medium-accuracy system (1 nm/hr, 1σ) with a baroaltitude-damped vertical channel. It employs three ring laser gyroscopes and three accelerometers, which have the characteristics indicated in Table 2.

The *D*oppler *v*elocity *s*ensor (DVS) employs a standard strapdown lambda 3-beam configuration [7] to measure aircraft velocity in aircraft body coordinates relative to the terrain surface. The primary time-correlated error in the measurement of the forward velocity component is a scale factor type error in the order of 1-2% (1σ), depending upon the terrain. The error in measuring the lateral velocity component principally results from an antenna boresight azimuth misalignment which is typically less than 1° (1σ). In addition to these time-correlated errors, there is also a

significant noise component to the DVS measurements of velocity; the level of noise is typically 1 m/s (1σ) for the forward velocity measurement, and 1.5 m/s (1σ) for the lateral velocity measurement. It is assumed that the DVS is only operated over land, so that additional errors introduced by the effects of sea currents and waves can be ignored.

The *air data sensors* (ADS) include a pressure transducer to measure static air pressure, and an air temperature probe to measure outside air temperature. This information is used to compute baroaltitude.

IMU Gyro Performance Characteristics	
Characteristic	Performance
Scale factor repeatability Bias repeatability G-sensitive drift repeatability	150 ppm (1σ) 0.2 °/hr (1σ) 0.2 °/hr/g (1σ)
IMU Accelerometer Performance Characteristics	
Characteristic	Performance
Scale factor repeatability Bias repeatability	200 ppm (1σ) 100 μg (1σ)

Table 1. IMU Gyro and Accelerometer Performance Characteristics.

INS Gyro Performance Characteristics	
Characteristic	Performance
Scale factor repeatability Bias repeatability Random drift	5 ppm (1σ) 0.01 °/hr (1σ) 0.003°/√ hr (1σ)
INS Accelerometer Performance Characteristics	
Characteristic	Performance
Scale factor repeatability Bias repeatability	50 ppm (1σ) 50 μg (1σ)

Table 2. INS Gyro and Accelerometer Performance Characteristics.

2.2 Processing Overview

Velocity and angular increments from the IMU are processed in a strapdown navigator algorithm which mechanizes the navigation equations in a wander azimuth frame. Since the IMU is mounted directly on the antenna, the strapdown algorithm fundamentally computes antenna attitude and heading, and velocity and position of a particular point at the IMU location. A lever arm correction is applied within the navigator to obtain estimates of the velocity and position of the antenna phase centre which is the point of interest for SAR motion compensation. The computed baroaltitude is used in a classical third-order damping loop to stabilize the strapdown vertical channel.

The strapdown navigator estimates of antenna phase centre motion are provided to a targetting algorithm during intervals of SAR imaging. The targetting algorithm initially computes a line-of-sight vector from the antenna phase centre to the target, using target information supplied from other parts of the SAR system. This line-of-sight vector is then updated throughout the imaging interval. At each point in time, the targetting algorithm calculates the component of the antenna phase centre velocity lying along the line-of-sight vector, and integrates this velocity component in time to obtain phase centre displacement along the line-of-sight. From this displacement, an appropriate value of phase correction is computed for each point in time, and applied to the radar signal returns to compensate for the spurious antenna motion.

The outputs of the strapdown navigator, along with information from the master INS and DVS, are supplied to a Kalman filter which estimates various system and sensor errors associated with these devices. The filter-estimated strapdown navigation errors and IMU instrument errors are fed back to the strapdown navigator algorithm and used there to correct the relevant quantities in a closed loop fashion. The net result of this Kalman filter implementation is that alignment of a Doppler-damped INS is continually transferred to the strapdown navigator.

3. OPTIMAL TOA KALMAN FILTER DESIGN

3.1 State Vector

The state vector in the optimal TOA Kalman filter design contains 26 states, representing all significant time-correlated errors. The state vector can be expressed as

$$\mathbf{x} = \begin{bmatrix} \mathbf{x}_M \\ \mathbf{x}_{INS} \\ \mathbf{x}_{DVS} \\ \mathbf{x}_S \\ \mathbf{x}_{IMU} \end{bmatrix} , \qquad (1)$$

where the subvectors $\mathbf{x}_M$ and $\mathbf{x}_S$ contain master INS system error states and strapdown navigator system error states respectively, $\mathbf{x}_{INS}$ and $\mathbf{x}_{IMU}$ contain states that represent INS and IMU instrument errors respectively, and $\mathbf{x}_{DVS}$ contains augmenting states that represent errors in the DVS. These 26 states are listed in Table 3. The error states modelled in $\mathbf{x}_M$ and $\mathbf{x}_S$ are defined as system-indicated values minus true values, while the instrument error quantities modelled in $\mathbf{x}_{INS}$, $\mathbf{x}_{IMU}$ and $\mathbf{x}_{DVS}$ are defined as factory-calibrated values minus true values.

3.2 Initial Covariance Matrix

The initial covariance matrix $\mathbf{P}_0$ for the state vector is expressed in terms of the initial estimation error $\tilde{\mathbf{x}}_0$ as

$$\mathbf{P}_0 = E[\tilde{\mathbf{x}}_0 \tilde{\mathbf{x}}_0^T] \quad , \qquad (2)$$

where "E" denotes expectation value, the superscript "T" indicates matrix transpose, and the initial estimation error is defined by

$$\tilde{\mathbf{x}}_0 = \hat{\mathbf{x}}_0 - \mathbf{x}_0 \quad , \tag{3}$$

with $\hat{\mathbf{x}}_0$ denoting the estimated value of $\mathbf{x}_0$, the true value of the initial state vector. The initial covariance matrix for this TOA system is expressed in terms of submatrices as

$$\mathbf{P}_0 = \begin{bmatrix} \mathbf{P}_{M_0} & \mathbf{0} & \mathbf{0} & \mathbf{P}_{M/S_0} & \mathbf{0} \\ \mathbf{0} & \mathbf{P}_{INS_0} & \mathbf{0} & \mathbf{0} & \mathbf{0} \\ \mathbf{0} & \mathbf{0} & \mathbf{P}_{DVS_0} & \mathbf{0} & \mathbf{0} \\ \mathbf{P}^T_{M/S_0} & \mathbf{0} & \mathbf{0} & \mathbf{P}_{S_0} & \mathbf{0} \\ \mathbf{0} & \mathbf{0} & \mathbf{0} & \mathbf{0} & \mathbf{P}_{IMU_0} \end{bmatrix} \quad , \tag{4}$$

where

$$\mathbf{P}_{M_0} = E[\tilde{\mathbf{x}}_{M_0}\tilde{\mathbf{x}}^T_{M_0}] \quad , \tag{5}$$

$$\mathbf{P}_{INS_0} = E[\tilde{\mathbf{x}}_{INS_0}\tilde{\mathbf{x}}^T_{INS_0}] \quad , \tag{6}$$

$$\mathbf{P}_{S_0} = E[\tilde{\mathbf{x}}_{S_0}\tilde{\mathbf{x}}^T_{S_0}] \quad , \tag{7}$$

$$\mathbf{P}_{IMU_0} = E[\tilde{\mathbf{x}}_{IMU_0}\tilde{\mathbf{x}}^T_{IMU_0}] \quad , \tag{8}$$

$$\mathbf{P}_{DVS_0} = E[\tilde{\mathbf{x}}_{DVS_0}\tilde{\mathbf{x}}^T_{DVS_0}] \quad , \tag{9}$$

$$\mathbf{P}_{M/S_0} = E[\tilde{\mathbf{x}}_{M_0}\tilde{\mathbf{x}}^T_{S_0}] \quad . \tag{10}$$

Subvector	State	Description	Coordinate Frame
$\mathbf{x}_M$	δR_{M_X}	master INS position error along X axis	Wander Azimuth[1]
	δR_{M_Y}	master INS position error along Y axis	
	δV_{M_X}	master INS velocity error along X axis	
	δV_{M_Y}	master INS velocity error along Y axis	
	ϕ_{M_X}	master INS platform misalignment about X axis	
	ϕ_{M_Y}	master INS platform misalignment about Y axis	
	ϕ_{M_Z}	master INS platform misalignment about Z axis	
$\mathbf{x}_{INS}$	A_{M_x}	master INS x accelerometer bias	Aircraft Body[2]
	A_{M_y}	master INS y accelerometer bias	
	G_{M_x}	master INS x gyro bias	
	G_{M_y}	master INS y gyro bias	
	G_{M_z}	master INS z gyro bias	
$\mathbf{x}_{DVS}$	δS	DVS forward scale factor error	Aircraft Body
	γ	DVS azimuth boresight error	
$\mathbf{x}_S$	δR_{S_X}	strapdown navigator position error along X axis	Wander Azimuth
	δR_{S_Y}	strapdown navigator position error along Y axis	
	δV_{S_X}	strapdown navigator velocity error along X axis	
	δV_{S_Y}	strapdown navigator velocity error along Y axis	
	ϕ_{S_X}	strapdown navigator platform misalignment about X axis	
	ϕ_{S_Y}	strapdown navigator platform misalignment about Y axis	
	ϕ_{S_Z}	strapdown navigator platform misalignment about Z axis	
$\mathbf{x}_{IMU}$	A_{S_x}	IMU x accelerometer bias	IMU Body[3]
	A_{S_y}	IMU y accelerometer bias	
	G_{S_x}	IMU x gyro bias	
	G_{S_y}	IMU y gyro bias	
	G_{S_z}	IMU z gyro bias	

[1] Wander azimuth frame: X,Y axes level, Z axis up
[2] Aircraft body frame: x axis forward, y axis out right wing, z axis down
[3] IMU body frame: x axis forward, z axis down, y axis oriented to form right-handed coordinate system

Table 3. Description of States for the Optimal TOA Kalman Filter.

The submatrix $\mathbf{P}_{M_0}$ is given by

$$\mathbf{P}_{M_0} = \begin{bmatrix} \sigma^2_{MR} & 0 & 0 & 0 & 0 & 0 & 0 \\ 0 & \sigma^2_{MR} & 0 & 0 & 0 & 0 & 0 \\ 0 & 0 & \sigma^2_{MV} & 0 & 0 & 0 & 0 \\ 0 & 0 & 0 & \sigma^2_{MV} & 0 & 0 & 0 \\ 0 & 0 & 0 & 0 & \sigma^2_{M\phi} & 0 & 0 \\ 0 & 0 & 0 & 0 & 0 & \sigma^2_{M\phi} & 0 \\ 0 & 0 & 0 & 0 & 0 & 0 & \sigma^2_{M\phi_Z} \end{bmatrix}, \quad (11)$$

where the variables are defined as follows:

σ^2_{MR} - the variance of the error in the initial estimates of δR_{M_X} and δR_{M_Y},

σ^2_{MV} - the variance of the error in the initial estimates of δV_{M_X} and δV_{M_Y},

$\sigma^2_{M\phi}$ - the variance of the error in the initial estimates of ϕ_{M_X} and ϕ_{M_Y},

$\sigma^2_{M\phi_Z}$ - the variance of the error in the initial estimate of ϕ_{M_Z}.

In this system, position, velocity, wander angle and heading in the IMU strapdown navigator are initialized to master INS values for these quantities. This implies that at filter initialization, the following relationships between estimation errors are true:

$$\begin{aligned} \delta\tilde{R}_{S_i} &= \delta\tilde{R}_{M_i}, \quad i = X,Y \\ \delta\tilde{V}_{S_i} &= \delta\tilde{V}_{M_i}, \quad i = X,Y \\ \tilde{\phi}_{S_Z} &= \tilde{\phi}_{M_Z} \end{aligned} \quad (12)$$

Strapdown navigator roll and pitch are initialized independently from the master INS values because the IMU is mounted on the stabilized antenna while the master INS is mounted on the airframe. This last point, together with the equations in Eq.(12), results in the following expressions for $\mathbf{P}_{S_0}$ and $\mathbf{P}_{M/S_0}$:

$$\mathbf{P}_{S_0} = \begin{bmatrix} \sigma^2_{MR} & 0 & 0 & 0 & 0 & 0 & 0 \\ 0 & \sigma^2_{MR} & 0 & 0 & 0 & 0 & 0 \\ 0 & 0 & \sigma^2_{MV} & 0 & 0 & 0 & 0 \\ 0 & 0 & 0 & \sigma^2_{MV} & 0 & 0 & 0 \\ 0 & 0 & 0 & 0 & \sigma^2_{S\phi} & 0 & 0 \\ 0 & 0 & 0 & 0 & 0 & \sigma^2_{S\phi} & 0 \\ 0 & 0 & 0 & 0 & 0 & 0 & \sigma^2_{M\phi_Z} \end{bmatrix}, \quad (13)$$

$$\mathbf{P}_{M/S_0} = \begin{bmatrix} \sigma^2_{MR} & 0 & 0 & 0 & 0 & 0 & 0 \\ 0 & \sigma^2_{MR} & 0 & 0 & 0 & 0 & 0 \\ 0 & 0 & \sigma^2_{MV} & 0 & 0 & 0 & 0 \\ 0 & 0 & 0 & \sigma^2_{MV} & 0 & 0 & 0 \\ 0 & 0 & 0 & 0 & 0 & 0 & 0 \\ 0 & 0 & 0 & 0 & 0 & 0 & 0 \\ 0 & 0 & 0 & 0 & 0 & 0 & \sigma^2_{M\phi_Z} \end{bmatrix}. \quad (14)$$

In Eq.(13), $\sigma^2_{S\phi}$ is defined as the variance of the error in the initial estimates of ϕ_{S_X} and ϕ_{S_Y}.

The submatrices $\mathbf{P}_{INS_0}$, $\mathbf{P}_{IMU_0}$ and $\mathbf{P}_{DVS_0}$ are expressed as

$$\mathbf{P}_{INS_0} = \begin{bmatrix} \sigma^2_{MAB} & 0 & 0 & 0 & 0 \\ 0 & \sigma^2_{MAB} & 0 & 0 & 0 \\ 0 & 0 & \sigma^2_{MGB} & 0 & 0 \\ 0 & 0 & 0 & \sigma^2_{MGB} & 0 \\ 0 & 0 & 0 & 0 & \sigma^2_{MGB} \end{bmatrix}, \quad (15)$$

$$\mathbf{P}_{IMU_0} = \begin{bmatrix} \sigma^2_{SAB} & 0 & 0 & 0 & 0 \\ 0 & \sigma^2_{SAB} & 0 & 0 & 0 \\ 0 & 0 & \sigma^2_{SGB} & 0 & 0 \\ 0 & 0 & 0 & \sigma^2_{SGB} & 0 \\ 0 & 0 & 0 & 0 & \sigma^2_{SGB} \end{bmatrix}, \quad (16)$$

$$\mathbf{P}_{DVS_0} = \begin{bmatrix} \sigma^2_{DSF} & 0 \\ 0 & \sigma^2_{DB} \end{bmatrix}. \quad (17)$$

In the above expressions, the variables are defined as:

σ^2_{MAB} - variance of the master INS accelerometer bias, as specified in Table 2,

σ^2_{MGB} - variance of the master INS gyro bias, as specified in Table 2,

σ^2_{SAB} - variance of the strapdown IMU accelerometer bias, as specified in Table 1,

σ^2_{SGB} - variance of the strapdown IMU gyro bias, as specified in Table 1,

σ^2_{DSF} - variance of the Doppler forward scale factor error, as specified in Section 2.1,

σ^2_{DB} - variance of the Doppler antenna azimuth boresight misalignment, as specified in Section 2.1.

3.3 State Dynamics

The continuous model for the error state dynamics has the standard form applicable to linear systems:

$$\dot{\mathbf{x}}(t) = \mathbf{F}(t)\mathbf{x}(t) + \mathbf{w}(t) \quad . \tag{18}$$

In the above equation, $\mathbf{w}(t)$ is a 26 element vector of zero-mean white noise processes. This noise vector has the same structure as the state vector, namely

$$\mathbf{w} = \begin{bmatrix} \mathbf{w}_M \\ \mathbf{w}_{INS} \\ \mathbf{w}_{DVS} \\ \mathbf{w}_S \\ \mathbf{w}_{IMU} \end{bmatrix} , \tag{19}$$

and $\mathbf{F}(t)$ is a 26 by 26 element matrix with the following structure:

$$\mathbf{F} = \begin{bmatrix} \mathbf{F}_M & \mathbf{F}_{M/INS} & \mathbf{0} & \mathbf{0} & \mathbf{0} \\ \mathbf{0} & \mathbf{F}_{INS} & \mathbf{0} & \mathbf{0} & \mathbf{0} \\ \mathbf{0} & \mathbf{0} & \mathbf{F}_{DVS} & \mathbf{0} & \mathbf{0} \\ \mathbf{0} & \mathbf{0} & \mathbf{0} & \mathbf{F}_S & \mathbf{F}_{S/IMU} \\ \mathbf{0} & \mathbf{0} & \mathbf{0} & \mathbf{0} & \mathbf{F}_{IMU} \end{bmatrix} , \tag{20}$$

where $\mathbf{F}_M$ and $\mathbf{F}_S$ are 7×7 matrices, $\mathbf{F}_{M/INS}$ is a 7×5 matrix, $\mathbf{F}_{S/IMU}$ is a 7×5 matrix, $\mathbf{F}_{INS}$ is a 5×5 matrix, $\mathbf{F}_{IMU}$ is a 5×5 matrix, and $\mathbf{F}_{DVS}$ is a 2×2 matrix. Using the expressions from Eqs.(1), (19) and (20) in Eq.(18), the system dynamics can be expressed in terms of the state subvectors as

$$\dot{\mathbf{x}}_M = \mathbf{F}_M \mathbf{x}_M + \mathbf{F}_{M/INS} \mathbf{x}_{INS} + \mathbf{w}_M \quad , \tag{21}$$

$$\dot{\mathbf{x}}_{INS} = \mathbf{F}_{INS} \mathbf{x}_{INS} + \mathbf{w}_{INS} \quad , \tag{22}$$

$$\dot{\mathbf{x}}_{DVS} = \mathbf{F}_{DVS} \mathbf{x}_{DVS} + \mathbf{w}_{DVS} \quad , \tag{23}$$

$$\dot{\mathbf{x}}_S = \mathbf{F}_S \mathbf{x}_S + \mathbf{F}_{S/IMU} \mathbf{x}_{IMU} + \mathbf{w}_S \quad , \tag{24}$$

$$\dot{\mathbf{x}}_{IMU} = \mathbf{F}_{IMU} \mathbf{x}_{IMU} + \mathbf{w}_{IMU} \quad . \tag{25}$$

The elements of $\mathbf{F}_M$ correspond to a true frame inertial error model [8] mechanized for a wander azimuth coordinate system that has its origin at the master INS, and that has X, Y, Z axes and wander angle α as depicted in Figure 2.

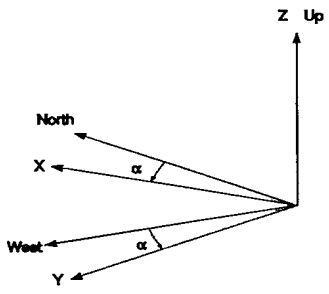

Figure 2. Orientation of Wander Azimuth Frame

This yields

$$\mathbf{F}_M = \begin{bmatrix} \frac{V_Z}{R_X} & 0 & 1 & 0 & 0 & 0 & 0 \\ 0 & \frac{V_Z}{R_Y} & 0 & 1 & 0 & 0 & 0 \\ F_{31} & F_{32} & -\frac{V_Z}{R_X} & 2\omega_{IE_Z} & 0 & -f_Z & f_Y \\ F_{41} & F_{42} & -2\omega_{IE_Z} & -\frac{V_Z}{R_Y} & f_Z & 0 & -f_X \\ -\frac{\omega_{IE_Z}}{R_X} & 0 & 0 & -\frac{1}{R_Y} & 0 & \omega_{IE_Z} & -\omega_{IW_Y} \\ 0 & -\frac{\omega_{IE_Z}}{R_Y} & \frac{1}{R_X} & 0 & -\omega_{IE_Z} & 0 & \omega_{IW_X} \\ \frac{\omega_{IW_X}}{R_X} & \frac{\omega_{IW_Y}}{R_Y} & 0 & 0 & \omega_{IW_Y} & -\omega_{IW_X} & 0 \end{bmatrix} \tag{26}$$

with $$F_{31} = \frac{V_Y}{R_X}(\omega_{IE_X} + \omega_{IW_X}) \quad ,$$

$$F_{32} = \frac{V_Y}{R_Y}(\omega_{IE_Y} + \omega_{IW_Y}) + 2\frac{V_Z}{R_y}\omega_{IE_Z} \quad ,$$

$$F_{41} = -\frac{V_X}{R_X}(\omega_{IE_Y} + \omega_{IW_X}) - 2\frac{V_Z}{R_X}\omega_{IE_Z} \quad ,$$

$$F_{42} = -\frac{V_X}{R_Y}(\omega_{IE_Y} + \omega_{IW_Y}) \quad ,$$

$$R_X = r_X + h \quad ,$$

$$R_Y = r_Y + h \quad .$$

In the above equation, the variables are defined as follows:

V_X, V_Y, V_Z - the X, Y, and Z components of **V**, the master INS velocity vector,

f_X, f_Y, f_Z - the X, Y, and Z components of **f**, the master INS specific force vector,

ω_{IE_X}, ω_{IE_Y}, ω_{IE_Z} - the X, Y, and Z components of ω_{IE}, the angular velocity vector of the earth with respect to inertial space,

ω_{IW_X}, ω_{IW_Y}, ω_{IW_Z} - the X, Y, and Z components of ω_{IW}, the angular velocity vector of the wander azimuth coordinate frame with respect to inertial space,

h - altitude of the master INS above the earth reference ellipsoid,

r_X, r_Y - local radii of curvature of the earth reference ellipsoid along the X and Y axes respectively.

Vertical channel error states for the master INS are not modelled in the Kalman filter because vertical channel errors are controlled with a third order fixed-gain damping loop implemented internally in the INS.

The elements of $\mathbf{F}_S$ have exactly the same form as that expressed in Eq.(26) for $\mathbf{F}_M$, except that the wander azimuth frame of interest has its origin at the strapdown IMU, and h, $\mathbf{V}$, and $\mathbf{f}$ apply to the strapdown IMU rather than the master INS.

The submatrix $\mathbf{F}_{M/INS}$ has the standard expression for a strapdown mechanization:

$$\mathbf{F}_{M/INS} = \begin{bmatrix} 0 & 0 & 0 & 0 & 0 \\ 0 & 0 & 0 & 0 & 0 \\ C_{11} & C_{12} & 0 & 0 & 0 \\ C_{21} & C_{22} & 0 & 0 & 0 \\ 0 & 0 & -C_{11} & -C_{12} & -C_{13} \\ 0 & 0 & -C_{21} & -C_{22} & -C_{23} \\ 0 & 0 & -C_{31} & -C_{32} & -C_{33} \end{bmatrix}, \quad (27)$$

where C_{ij} is the element in the ith row and jth column of the direction cosine matrix $\mathbf{C}_A^{MW}$ which expresses the transformation from the aircraft body frame to the master INS wander azimuth frame. The aircraft body frame is defined in Table 3. $\mathbf{C}_A^{MW}$ is computed as

$$\mathbf{C}_A^{MW} = \begin{bmatrix} \cos A\cos P & -\sin A\cos R + \cos A\sin P\sin R & \sin A\sin R + \cos A\sin P\cos R \\ -\sin A\cos P & -\cos A\cos R - \sin A\sin P\sin R & \cos A\sin R - \sin A\sin P\cos R \\ \sin P & -\cos P\sin R & -\cos P\cos R \end{bmatrix} \quad (28)$$

with

$$A = \alpha + H \quad ,$$

and the variables defined as:

α - wander angle for the master INS wander angle frame,

R - aircraft roll,

P - aircraft pitch,

H - aircraft heading from North.

The submatrix $\mathbf{F}_{S/IMU}$ has exactly the same form as $\mathbf{F}_{M/INS}$ in Eq.(27) except that in the case of $\mathbf{F}_{S/IMU}$, the C_{ij} are elements of the direction cosine matrix $\mathbf{C}_B^{SW}$ which describes the transformation from the strapdown IMU body frame to the wander azimuth frame centered at the IMU. The strapdown IMU body frame is described in Table 3. $\mathbf{C}_B^{SW}$ is given by the same expression as in Eq.(28) with roll, pitch and heading interpreted as being that of the IMU. In general, the roll and pitch of the strapdown IMU is close to zero, since the IMU is mounted on the antenna which is physically stabilized in roll and pitch.

The dynamics of the error states in $\mathbf{x}_{INS}$, $\mathbf{x}_{IMU}$, and $\mathbf{x}_{DVS}$ are modelled as first order Markov processes, resulting in the following submatrices:

$$\mathbf{F}_{INS} = \begin{bmatrix} -\beta_{MAB} & 0 & 0 & 0 & 0 \\ 0 & -\beta_{MAB} & 0 & 0 & 0 \\ 0 & 0 & -\beta_{MGB} & 0 & 0 \\ 0 & 0 & 0 & -\beta_{MGB} & 0 \\ 0 & 0 & 0 & 0 & -\beta_{MGB} \end{bmatrix}, \quad (29)$$

$$\mathbf{F}_{IMU} = \begin{bmatrix} -\beta_{SAB} & 0 & 0 & 0 & 0 \\ 0 & -\beta_{SAB} & 0 & 0 & 0 \\ 0 & 0 & -\beta_{SGB} & 0 & 0 \\ 0 & 0 & 0 & -\beta_{SGB} & 0 \\ 0 & 0 & 0 & 0 & -\beta_{SGB} \end{bmatrix}, \quad (30)$$

$$\mathbf{F}_{DVS} = \begin{bmatrix} -\beta_{DSF} & 0 \\ 0 & -\beta_{DB} \end{bmatrix} . \quad (31)$$

In Eqs.(29) to (31), the variables are defined as:

β_{MAB} - inverse of the correlation time for the master INS accelerometer bias error,

β_{MGB} - inverse of the correlation time for the master INS gyro bias error,

β_{SAB} - inverse of the correlation time for the strapdown IMU accelerometer bias error,

β_{SGB} - inverse of the correlation time for the strapdown IMU gyro bias error,

β_{DSF} - inverse of the correlation time for the DVS forward scale factor error,

β_{DB} - inverse of the correlation time for the DVS azimuth boresight error.

The vector of random forcing functions in Eq.(18), denoted by $\mathbf{w}$, is described in terms of its covariance matrix which is given in the continuous formulation by

$$\mathbf{P}_w = E[\mathbf{w}(t)\mathbf{w}(\tau)^T] = \mathbf{Q}(t)\delta(t-\tau) \quad , \quad (32)$$

where $\delta(t-\tau)$ is the Dirac delta function and $\mathbf{Q}(t)$ is a spectral density matrix. For this system, $\mathbf{Q}$ is expressed in terms of submatrices as

$$\mathbf{Q} = \begin{bmatrix} \mathbf{Q}_M & \mathbf{0} & \mathbf{0} & \mathbf{Q}_{M/S} & \mathbf{0} \\ \mathbf{0} & \mathbf{Q}_{INS} & \mathbf{0} & \mathbf{0} & \mathbf{0} \\ \mathbf{0} & \mathbf{0} & \mathbf{Q}_{DVS} & \mathbf{0} & \mathbf{0} \\ \mathbf{Q}_{M/S}^T & \mathbf{0} & \mathbf{0} & \mathbf{Q}_S & \mathbf{0} \\ \mathbf{0} & \mathbf{0} & \mathbf{0} & \mathbf{0} & \mathbf{Q}_{IMU} \end{bmatrix} . \quad (33)$$

In the above equation, the submatrix $\mathbf{Q_M}$ is given by:

$$\mathbf{Q_M} = \begin{bmatrix} 0 & 0 & 0 & 0 & 0 & 0 & 0 \\ 0 & 0 & 0 & 0 & 0 & 0 & 0 \\ 0 & 0 & q_{VD} + q_{MASF} & 0 & 0 & 0 & 0 \\ 0 & 0 & 0 & q_{VD} + q_{MASF} & 0 & 0 & 0 \\ 0 & 0 & 0 & 0 & q_{MGN} & 0 & 0 \\ 0 & 0 & 0 & 0 & 0 & q_{MGN} & 0 \\ 0 & 0 & 0 & 0 & 0 & 0 & q_{MGN} \end{bmatrix} , \quad (34)$$

where q_{VD} and q_{MASF} are the spectral densities of white noise models to account for the effects of vertical deflections and INS accelerometer scale factor errors respectively, and q_{MGN} is the spectral density of the white noise associated with the random drift of the INS ring laser gyros, as specified in Table 2. The spectral densities q_{VD} and q_{MASF} are given by the expressions

$$q_{VD} = \frac{2 d_{VD} g^2}{V_g} \sigma^2_{VD} \quad , \quad (35)$$

$$q_{MASF} = \frac{4 V_g a}{\pi} \sigma^2_{MASF} \quad , \quad (36)$$

where the variables have the following definitions:

g - the nominal value of gravity,

d_{VD} - the correlation distance of the random deflections of the vertical,

σ^2_{VD} - the variance of the deflections of the vertical,

V_g - aircraft ground speed,

a - magnitude of the aircraft acceleration vector,

σ^2_{MASF} - the variance of the master INS accelerometer scale factor error, as indicated in Table 2.

A derivation for the expressions in Eqs.(35) and (36) is given in [9].

The submatrix $\mathbf{Q_g}$ is written as:

$$\mathbf{Q_g} = \begin{bmatrix} 0 & 0 & 0 & 0 & 0 & 0 & 0 \\ 0 & 0 & 0 & 0 & 0 & 0 & 0 \\ 0 & 0 & q_{VD} + q_{SASF} & 0 & 0 & 0 & 0 \\ 0 & 0 & 0 & q_{VD} + q_{SASF} & 0 & 0 & 0 \\ 0 & 0 & 0 & 0 & q_{SGMU} & 0 & 0 \\ 0 & 0 & 0 & 0 & 0 & q_{SGMU} & 0 \\ 0 & 0 & 0 & 0 & 0 & 0 & q_{SGMU} + q_{SGSF} \end{bmatrix} , \quad (37)$$

where q_{VD} is as defined previously, and q_{SASF}, q_{SGMU} and q_{SGSF} are the spectral densities of white noise models that account for the effects of strapdown IMU accelerometer scale factor errors, IMU gyro mass unbalances excited by aircraft accelerations, and the z gyro scale factor error respectively. Of course, gyro mass unbalances are also excited by the constant gravitational field, but this component of the mass unbalance effect is indistinguishable from a gyro bias effect and so is lumped in with the modelled gyro bias states. It should also be noted that the effects of the IMU x and y gyro scale factor errors are not modelled because in this case, these errors do not contribute to inertial platform misalignments; since the x and y gyro input axes are physically stabilized in the horizontal plane, they do not experience any significant angular velocities that would excite scale factor error effects. On the other hand, the z gyro input axis, which essentially points along the local vertical, does experience a significant angular velocity during an aircraft heading change, so that during a turn, the z gyro scale factor error causes a platform misalignment about the Z wander azimuth axis.

The spectral densities q_{SASF}, q_{SGMU} and q_{SGSF} are given by the expressions:

$$q_{SASF} = \frac{4 V_g a}{\pi} \sigma^2_{SASF} \quad , \quad (38)$$

$$q_{SGMU} = \frac{4 V_g a}{\pi} \sigma^2_{SGMU} \quad , \quad (39)$$

$$q_{SGSF} = \pi \left|\omega_z\right| \sigma^2_{SGSF} \quad , \quad (40)$$

where the variables have the following definitions:

σ^2_{SASF} - the variance of the IMU accelerometer scale factor error, as specified in Table 1,

σ^2_{SGMU} - the variance of the strapdown IMU gyro mass unbalance, as specified in Table 1,

σ^2_{SGSF} - the variance of the strapdown IMU gyro scale factor error, as specified in Table 1,

$\left|\omega_z\right|$ - the magnitude of the z IMU body axis component of the IMU angular rate vector.

Derivations for the expressions in Eqs.(38) to (40) are found in [9].

The submatrix $\mathbf{Q}_{M/S}$ is defined by the equation

$$\mathbf{Q}_{M/S}(t)\delta(t-\tau) = E[\mathbf{w}_M(t)\mathbf{w}_S(\tau)^T] \quad (41)$$

and is given by

$$\mathbf{Q}_{M/S} = \begin{bmatrix} 0 & 0 & 0 & 0 & 0 & 0 & 0 \\ 0 & 0 & 0 & 0 & 0 & 0 & 0 \\ 0 & 0 & q_{VD} & 0 & 0 & 0 & 0 \\ 0 & 0 & 0 & q_{VD} & 0 & 0 & 0 \\ 0 & 0 & 0 & 0 & 0 & 0 & 0 \\ 0 & 0 & 0 & 0 & 0 & 0 & 0 \\ 0 & 0 & 0 & 0 & 0 & 0 & 0 \end{bmatrix} . \quad (42)$$

In the above expression, the two non-zero terms along the diagonal represent the correlation that exists between elements of $\mathbf{w}_M$ and $\mathbf{w}_S$ as a result of modelling vertical deflection effects as a white noise process that drives both the master INS and strapdown navigator velocity error states.

The submatrices $\mathbf{Q}_{INS}$, $\mathbf{Q}_{IMU}$, and $\mathbf{Q}_{DVS}$ are

$$\mathbf{Q}_{INS} = \begin{bmatrix} q_{MAB} & 0 & 0 & 0 & 0 \\ 0 & q_{MAB} & 0 & 0 & 0 \\ 0 & 0 & q_{MGB} & 0 & 0 \\ 0 & 0 & 0 & q_{MGB} & 0 \\ 0 & 0 & 0 & 0 & q_{MGB} \end{bmatrix} , \quad (43)$$

$$\mathbf{Q}_{IMU} = \begin{bmatrix} q_{SAB} & 0 & 0 & 0 & 0 \\ 0 & q_{SAB} & 0 & 0 & 0 \\ 0 & 0 & q_{SGB} & 0 & 0 \\ 0 & 0 & 0 & q_{SGB} & 0 \\ 0 & 0 & 0 & 0 & q_{SGB} \end{bmatrix} , \quad (44)$$

$$\mathbf{Q}_{DVS} = \begin{bmatrix} q_{DSF} & 0 \\ 0 & q_{DB} \end{bmatrix} . \quad (45)$$

The spectral densities in the expressions above are computed from the following expressions:

$$q_{MAB} = 2\sigma^2_{MAB}\beta_{MAB} , \quad (46)$$

$$q_{MGB} = 2\sigma^2_{MGB}\beta_{MGB} , \quad (47)$$

$$q_{SAB} = 2\sigma^2_{SAB}\beta_{SAB} , \quad (48)$$

$$q_{SGB} = 2\sigma^2_{SGB}\beta_{SGB} , \quad (49)$$

$$q_{DSF} = 2\sigma^2_{DSF}\beta_{DSF} , \quad (50)$$

$$q_{DB} = 2\sigma^2_{DB}\beta_{DB} , \quad (51)$$

where all variables have been previously defined. The spectral density expressions in Eqs.(46) through to (51) represent the level of driving white noise for each Markov process model that results in the steady-state variances for the models being equal to the initial estimation error variances described in Section 3.2.

From the description of the state vector and state dynamics model given in this section, it is clear that even this so-called "optimal" design is not truly optimal, in the sense that certain simplifying assumptions have already been made to restrict the number of modelled states. The model simplifications include the following:

1) Vertical position error, vertical velocity error and vertical accelerometer bias states have not been modelled in the Kalman filter for either the master INS or the IMU strapdown navigator because these errors are kept small by separate fixed-gain baroaltitude damping loops.

2) The effect of the scale factor error in the master INS ring laser gyros has not been modelled because it is very small (5 ppm) and its effect is expected to be insignificant compared to the effect of other master INS gyro errors.

3) Certain time-correlated errors in the strapdown IMU sensors, such as gyro mass unbalances and gyro scale factor errors, have only been modelled, if at all, as white noise processes driving the inertial system error states, because for this configuration where the IMU is physically stabilized in roll and pitch, their effects are too small to allow these errors to be observable as separately modelled states in the Kalman filter.

4) Vertical deflection effects have been modelled as a white noise process driving velocity error states because these effects are expected to be too small to warrant modelling as filter states.

Whether or not a filter designer feels confident in making such model simplifications right at the outset of the design process depends largely on the designer's experience and understanding of the system at hand. Typically, it is desireable to make some initial model simplifications simply to reduce the development time required to arrive at the final Kalman filter configuration. However, if there is any doubt as to the significance of certain errors, it is better to err on the side of caution and include them as modelled states in the initial filter design. Later, through further analysis, detailed simulations and field trials, the designer gains additional insights into the system error behaviour, which may then allow him to reduce the model complexity with a higher degree of confidence. The initial filter formulation then serves as the designer's "optimal" configuration against which the performance of other more suboptimal designs is compared. In this respect, the state dynamics model presented in this section is considered the optimal Kalman filter model for the TOA system, despite containing the model simplifications described.

3.4 Measurements

Two different sets of measurements are constructed for use in the Kalman filter. One set is a velocity matching measurement $\mathbf{z}_D$ between the DVS and the master INS. This

measurement type is used to estimate velocity and attitude errors in the master INS. The other set is a velocity matching measurement $\mathbf{z}_V$ between the master INS and the strapdown navigator, which effectively accomplishes the transfer of alignment.

The measurement vector $\mathbf{z}_D$ is computed as

$$\begin{aligned}\mathbf{z}_D^A &= \begin{bmatrix} z_{D_x} & z_{D_y} & z_{D_z} \end{bmatrix}^T \\ &= (\mathbf{C}_A^{MW^T}\mathbf{V}_M^{MW} - \mathbf{V}_D^A) + (\boldsymbol{\omega}_A^A \times \mathbf{d}_D^A) \quad ,\end{aligned} \tag{52}$$

where the variables are defined as follows:

$\mathbf{z}_D^A$ - the master INS/Doppler measurement vector resolved in the aircraft body frame, denoted by the superscript "A",

$\mathbf{C}_A^{MW}$ - the direction cosine matrix computed from Eq.(28) by using the roll, pitch, heading and wander angle indicated by the master INS,

$\mathbf{V}_M^{MW}$ - the velocity vector computed by the master INS and resolved in the master wander azimuth frame, as denoted by the superscript "MW",

$\mathbf{V}_D^A$ - the aircraft velocity vector indicated by the DVS and resolved in the aircraft body frame,

$\boldsymbol{\omega}_A^A$ - the angular velocity vector of the aircraft body frame with respect to an earth-fixed frame, as computed by the master INS, resolved in the aircraft body frame,

$\mathbf{d}_D^A$ - the lever arm vector from the master INS to the DVS, resolved in the aircraft body frame.

The measurement vector $\mathbf{z}_V$ is calculated by the expression

$$\begin{aligned}\mathbf{z}_V^{MW} &= [z_{V_X} \quad z_{V_Y} \quad z_{V_Z}]^T \\ &= (\mathbf{C}_{SW}^{MW}\mathbf{V}_S^{SW} - \mathbf{V}_M^{MW}) - (\mathbf{C}_A^{MW}[\boldsymbol{\omega}_A^A \times \mathbf{d}_S^A]) \quad ,\end{aligned} \tag{53}$$

where the variables not previously defined are :

$\mathbf{z}_V^{MW}$ - the master INS/strapdown measurement vector, resolved in the master INS wander azimuth frame,

$\mathbf{V}_S^{SW}$ - velocity vector computed by the IMU strapdown navigator, and resolved in the strapdown IMU wander azimuth frame, denoted by the superscript "SW",

$\mathbf{d}_S^A$ - the lever arm vector from the master INS to the strapdown IMU, resolved in the aircraft body frame,

$\mathbf{C}_{SW}^{MW}$ - the direction cosine matrix describing the transformation from the strapdown IMU wander azimuth frame to the master INS wander azimuth frame.

The matrix $\mathbf{C}_{SW}^{MW}$ is computed by

$$\mathbf{C}_{SW}^{MW} = \mathbf{C}_{MW}^{E^T}\mathbf{C}_{SW}^{E} \quad , \tag{54}$$

where $\mathbf{C}_{SW}^{E}$ and $\mathbf{C}_{MW}^{E}$ are the direction cosine matrices describing respectively the transformation from the strapdown IMU wander azimuth frame to a specified earth-fixed frame, and the transformation from the master INS wander azimuth frame to the earth-fixed frame. The matrix $\mathbf{C}_{SW}^{E}$ is calculated as

$$\mathbf{C}_{SW}^{E} = \begin{bmatrix} \cos\alpha\cos L & -\sin\alpha\cos L & \sin L \\ \sin\alpha\cos l + \cos\alpha\sin L\sin l & \cos\alpha\cos l - \sin\alpha\sin L\sin l & -\cos L\sin l \\ \sin\alpha\sin l - \cos\alpha\sin L\cos l & \cos\alpha\sin l + \sin\alpha\sin L\cos l & \cos L\cos l \end{bmatrix} , \tag{55}$$

where α, L and l are the wander angle, latitude and longitude computed by the IMU strapdown navigator. The matrix $\mathbf{C}_{MW}^{E}$ is calculated with exactly the same expression as in Eq.(55) except that the wander angle, latitude and longitude used are those indicated by the master INS.

The Kalman filter actually processes only z_{V_X} and z_{V_Y}, the horizontal components of $\mathbf{z}_V^{MW}$, and z_{D_x} and z_{D_y}, the x and y components of $\mathbf{z}_D^A$. Also, the master INS/Doppler measurements are processed only during nominally straight and level flight to avoid additional inaccuracies in the DVS that result when the aircraft is steeply rolled or pitched. The measurement vector $\mathbf{z}$ that is processed by the filter is then written as

$$\mathbf{z} = \begin{bmatrix} z_{D_x} \\ z_{D_y} \\ z_{V_X} \\ z_{V_Y} \end{bmatrix} . \tag{56}$$

3.5 Measurement Models

The linear model for discrete measurements is given by

$$\mathbf{z} = \mathbf{H}\mathbf{x} + \mathbf{v} \quad , \tag{57}$$

where $\mathbf{H}$ is the measurement matrix with dimension 4×26 and $\mathbf{v}$ is a 4 element vector of measurement errors that are assumed to be zero-mean sequences uncorrelated in time. The measurement matrix is derived by perturbing the right hand side of Eqs.(52) and (53) and expressing the result in terms of the modelled error states. The following assumptions are made in this derivation: 1) the effect of errors in computing the $\boldsymbol{\omega}\times\mathbf{d}$ terms and the transformation matrix $\mathbf{C}_{SW}^{MW}$ can be neglected (these small effects are included in the measurement noise model), 2) the x and y axes of the aircraft body frame are nominally in the horizontal plane when master INS/Doppler measurements are constructed, which allows the measurement error terms containing vertical velocity errors to be neglected, and 3) vertical velocities are small enough (i.e. < 10 m/s) to allow measurement error terms containing vertical velocity to be neglected. These last two assumptions are valid since, as

pointed out earlier, master INS/Doppler measurements are processed only during nominally straight and level flight. The resulting measurement matrix is expressed in terms of submatrices as:

$$\mathbf{H} = \begin{bmatrix} \mathbf{H}_{D_M} & \mathbf{0} & \mathbf{H}_{D_{DVS}} & \mathbf{0} & \mathbf{0} \\ \mathbf{H}_{V_M} & \mathbf{0} & \mathbf{0} & \mathbf{H}_{V_S} & \mathbf{0} \end{bmatrix} . \quad (58)$$

The submatrices $\mathbf{H}_{D_M}$ and $\mathbf{H}_{D_{DVS}}$, which have dimensions of 2×7 and 2×2 respectively, are given by

$$\mathbf{H}_{D_M} = \begin{bmatrix} 0 & 0 & C_{11} & C_{21} & C_{31}V_{M_Y} & -C_{31}V_{M_X} & (C_{21}V_{M_X} - C_{11}V_{M_Y}) \\ 0 & 0 & C_{12} & C_{22} & C_{32}V_{M_Y} & -C_{32}V_{M_X} & (C_{22}V_{M_X} - C_{12}V_{M_Y}) \end{bmatrix} \quad (59)$$

$$\mathbf{H}_{D_{DVS}} = \begin{bmatrix} -V_{D_x} & 0 \\ 0 & V_{D_x} \end{bmatrix} , \quad (60)$$

where the variables are defined as:

C_{ij} - the elements of $\mathbf{C}_A^{MW}$,

V_{D_x} - the x component of $\mathbf{V}_D^A$

V_{M_X}, V_{M_Y} - the X and Y components of $\mathbf{V}_M^{MW}$,

V_{M_x}, V_{M_y} - the x and y components of $\mathbf{V}_M^A$ which is computed as

$$\mathbf{V}_M^A = \mathbf{C}_A^{MW^T}\mathbf{V}_M^{MW} . \quad (61)$$

The submatrices $\mathbf{H}_{V_M}$ and $\mathbf{H}_{V_S}$, both of dimension 2×7, are given below:

$$\mathbf{H}_{V_M} = \begin{bmatrix} 0 & 0 & -1 & 0 & 0 & 0 & 0 \\ 0 & 0 & 0 & -1 & 0 & 0 & 0 \end{bmatrix} , \quad (62)$$

$$\mathbf{H}_{V_S} = \begin{bmatrix} 0 & 0 & C'_{11} & C'_{12} & 0 & 0 & 0 \\ 0 & 0 & C'_{21} & C'_{21} & 0 & 0 & 0 \end{bmatrix} , \quad (63)$$

where the C'_{ij} are the elements of $\mathbf{C}_{SW}^{MW}$.

The measurement noise vector $\mathbf{v}$ is characterized by its covariance matrix $\mathbf{R}$ which is given by

$$\mathbf{R} = E[\mathbf{v}\,\mathbf{v}^T] = \begin{bmatrix} \sigma_{D_x}^2 & 0 & 0 & 0 \\ 0 & \sigma_{D_y}^2 & 0 & 0 \\ 0 & 0 & \sigma_V^2 & 0 \\ 0 & 0 & 0 & \sigma_V^2 \end{bmatrix} . \quad (64)$$

In the above equation, the variables are defined as

$\sigma_{D_x}^2$ - the variance of the measurement noise for z_{D_x},

$\sigma_{D_y}^2$ - the variance of the measurement noise for z_{D_y},

σ_V^2 - the variance of the measurement noise for z_{V_X} and z_{V_Y}.

The main contributor to the measurement noise for z_{D_x} and z_{D_y} is the noise on the DVS velocity measurements, which is specified in Section 2.1. The measurement noise modelled for z_{V_X} and z_{V_Y} includes the effects of quantization of master INS velocity data, and the effects of airframe flexing which causes errors in computing relative velocity between the master INS and strapdown IMU.

The fact that the matrix $\mathbf{R}$ is diagonal implies that the elements of $\mathbf{v}$ are uncorrelated with each other. Strictly speaking, this is not true. There is a correlation between the measurement noise for z_{D_x} and z_{D_y} due to the fact that the noise associated with the DVS forward and lateral velocity measurements is somewhat correlated. However, by assuming that the noise elements are uncorrelated, there is only a small loss in optimality, while there is a significant advantage gained in that the scalar components of the measurement vector can be processed sequentially by the filter at a given update time, rather than processing the $\mathbf{z}$ vector as a whole. This allows matrix inversion to be avoided, thereby increasing computational efficiency.

3.6 Simulation Results

A high-fidelity computer simulation is an extremely useful tool in evaluating a Kalman filter design and predicting filter performance. Such a simulation was performed for the optimal TOA filter described in this section.

The simulation package that was used generates simulated master INS, strapdown IMU, DVS and air data, which are then used as inputs to a processing package. The simulated sensor data corresponds to a particular user-defined flight profile, and includes the effects of all the sensor errors discussed in Section 2.1, as well as other errors like quantization of the sensor output data. The simulation package also provides files containing true position, velocity, attitude and heading as a function of time for both the master INS and strapdown IMU. These files serve as the reference against which the processing package outputs are compared in order to evaluate Kalman filter estimation errors. The processing package consists of the Kalman filter, strapdown navigator and baroaltitude algorithm shown in the block diagram of Figure 1.

For the Kalman filter processor, the Kalman filter equations are implemented in their discrete form using Bierman's U-D factorization algorithm [10] to efficiently propagate and update the error covariance matrix . Other features that are used to enhance computational efficiency include sequential processing of measurements, sparse matrix multiplication techniques and exploitation of the block structure of certain matrices to increase the execution speed of matrix operations. In the discrete Kalman filter formulation, the model for the error state dynamics as expressed in Eq.(18) is converted to a discrete-time model of the form:

$$\mathbf{x}_{k+1} = \Phi_k \mathbf{x}_k + \mathbf{w}_k \quad , \tag{65}$$

where $\mathbf{w}_k$ is a vector of zero-mean white noise sequences with covariance matrix $\mathbf{Q}_k$, and $\mathbf{x}_k$ and $\mathbf{x}_{k+1}$ refer to the values of the state vector at times t_k and t_{k+1} respectively. The interval $\Delta T_k \equiv (t_{k+1} - t_k)$ is the interval between Kalman filter measurement updates. The update interval for this simulation is 10 seconds. To obtain the transition matrix Φ_k, a transition matrix Φ_j is first computed over a smaller subinterval, referred to as the propagation interval, by retaining the first three terms of the matrix exponential expression below:

$$\begin{aligned}\Phi_j &= \exp(\overline{\mathbf{F}}_j \Delta t_j) \\ &= \mathbf{I} + \overline{\mathbf{F}}_j \Delta t_j + \frac{1}{2}\overline{\mathbf{F}}_j^2 (\Delta t_j)^2 + \frac{1}{6}\overline{\mathbf{F}}_j^3 (\Delta t_j)^3 + \ldots \quad ,\end{aligned} \tag{66}$$

where Δt_j is the propagation interval defined by $\Delta t_j \equiv (t_{j+1} - t_j)$, and $\overline{\mathbf{F}}_j$ is the average value of $\mathbf{F}(t)$ over Δt_j, with $\mathbf{F}(t)$ given by the expression in Eq.(20). In the simulation, the basic propagation interval is 2 seconds. The transition matrix Φ_j is recalculated every propagation interval, and Φ_k is then calculated as

$$\Phi_k = \Phi_{j+4}\Phi_{j+3}\Phi_{j+2}\Phi_{j+1}\Phi_j \quad . \tag{67}$$

The covariance matrix $\mathbf{Q}_k$ is computed from the expression

$$\mathbf{Q}_k = \int_0^{\Delta T_k} e^{\mathbf{F}_{k+1}\tau} \mathbf{Q}(\tau) (e^{\mathbf{F}_{k+1}\tau})^T \, d\tau \tag{68}$$

by expanding the matrix exponential terms, multiplying out and integrating the products with the assumption that $\mathbf{Q}(t)$, the spectral density matrix given in Eq.(33), is constant over the interval ΔT_k. In the above expression, $\mathbf{F}_{k+1}$ is the value of $\mathbf{F}(t)$ at t_{k+1}.

For this simulation, the elements of the submatrices $\mathbf{P}_{M_0}$ and $\mathbf{P}_{S_0}$ in the initial error covariance matrix $\mathbf{P}_0$ were assigned values consistent with expected system errors in the INS following a stationary ground alignment. The flight profile used for the simulation is depicted in Figure 3. A description of the various manoeuvres included in the simulated flight profile is given in Table 4. It should be noted that the DVS data is not used to construct Kalman filter measurements until cruising altitude is reached. The velocity matching measurements between the strapdown navigator and master INS are constructed and processed right from time zero.

The performance of the optimal TOA Kalman filter is indicated in Figures 4 to 8. The solid traces in the plots indicate the strapdown navigator velocity, attitude and heading estimation errors over the course of the flight, assuming closed loop correction of strapdown navigator quantities with the filter-estimated error states. The estimation errors are obtained by subtracting the "true" velocity, attitude and heading values, as generated by the simulation package, from the corresponding values computed by the strapdown navigator in the processing package. The dashed lines show the filter-predicted standard deviation bounds for these estimation errors. The sharp decreases in the standard deviation bounds generally occur right after turns, when DVS error states and inertial platform misalignments about the Z axis become separately observable from the other error states. It can be seen that the time histories of the estimation errors are fairly consistent with the predicted standard deviation bounds.

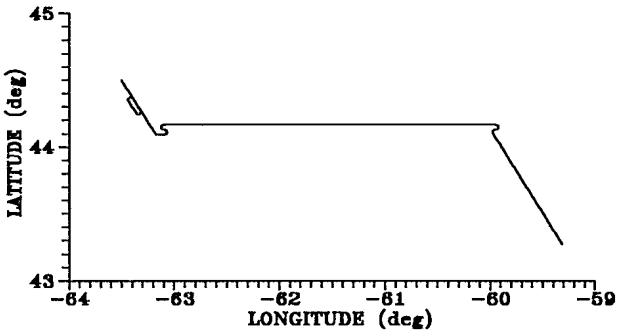

Figure 3. Simulated Flight Profile

TIME (s)	DESCRIPTION OF MANOEUVRE
0	Stationary; heading is 150 degrees
3	Start accelerating down runway
75	Takeoff; aircraft pitch increases to 6 degrees
116	Achieve and maintain cruising speed of 108 m/s
173	Reach and maintain cruising altitude of 1000 m; aircraft pitch returns to zero
330	Enter racetrack; aircraft roll increases to 30 degrees
392	Complete first 180 degree turn of racetrack
500	Enter second turn of racetrack
562	Complete second 180 degree turn of racetrack; aircraft heading returns to 150 degrees
870	Start turn to heading of 90 degrees
891	Complete turn to heading of 90 degrees
941	Start S-manoeuvre
1067	Complete S-manoeuvre; aircraft heading returns to 90 degrees
3400	Start S-manoeuvre
3506	Complete S-manoeuvre; heading held at 150 degrees
4500	Complete profile

Table 4. Description of Manoeuvres in Simulated Flight Profile.

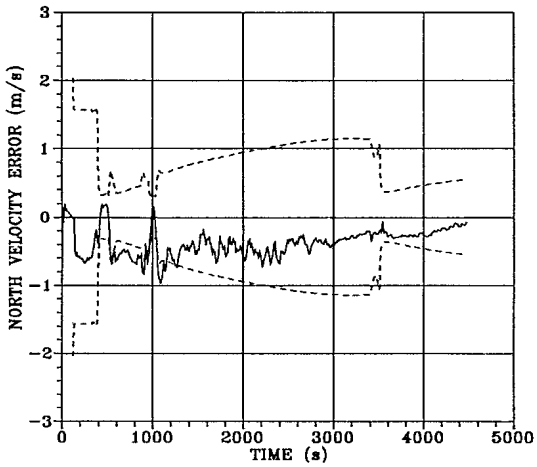

Figure 4. Strapdown Navigator North Velocity Error and Predicted Error Standard Deviation (Optimal Filter).

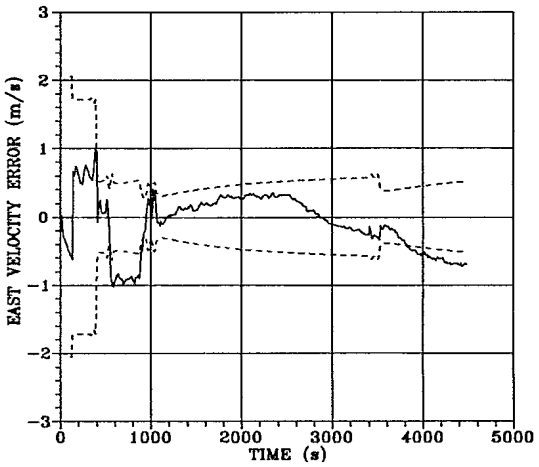

Figure 5. Strapdown Navigator East Velocity Error and Predicted Error Standard Deviation (Optimal Filter).

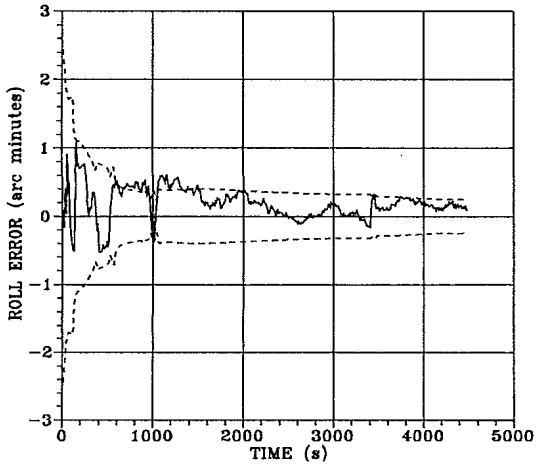

Figure 6. Strapdown Navigator Roll Error and Predicted Error Standard Deviation (Optimal Filter).

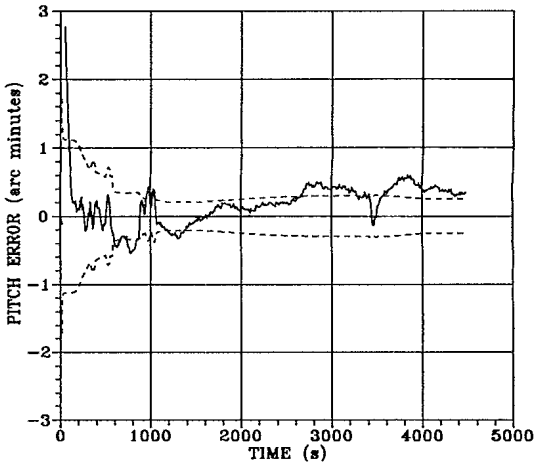

Figure 7. Strapdown Navigator Pitch Error and Predicted Error Standard Deviation (Optimal Filter).

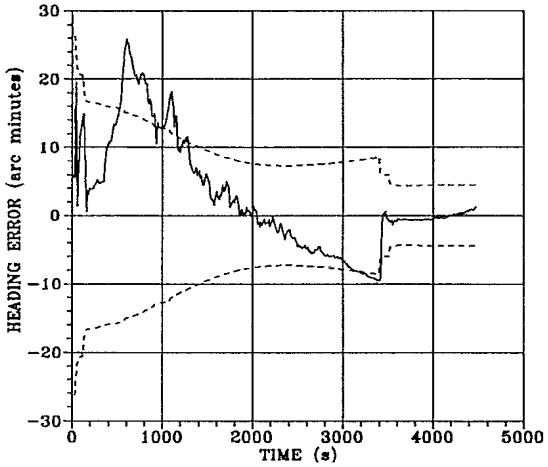

Figure 8. Strapdown Navigator Heading Error and Predicted Error Standard Deviation (Optimal Filter).

4. SUBOPTIMAL TOA KALMAN FILTER DESIGN

4.1 State Decoupling

If certain parts of a system state vector are only weakly coupled, it is often possible to split the one Kalman filter into two or more lower order filters. This can reduce the computational burden by a significant amount since the number of multiplications required to perform the most intensive filter task - the solution of the error covariance equations - varies roughly as the third power of the number of states.

In this section, it is shown that the optimal TOA Kalman filter described in Section 3 can effectively be split into two filters. The Doppler damping of the master INS is performed in one filter, while the transfer of alignment from the master INS to the strapdown navigator is performed in a second filter which is mathematically decoupled from the first.

The means by which the original Kalman filter can be decoupled becomes more apparent if one considers an alternate filter formulation for which the *differences* between the absolute errors in the master INS and strapdown navigator are modelled, instead of the absolute strapdown navigator errors themselves. Such a filter formulation is based on the fundamental insight that measurements constructed by comparing equivalent information from two systems with the same error dynamics will only allow differences between the two systems to be observable, rather than the absolute errors in each system. Thus the velocity matching measurement between the master INS and strapdown navigator provides direct observability only for $\mathbf{x}'_s$ where

$$\mathbf{x}'_s = \mathbf{x}_s - \mathbf{x}_M = \begin{bmatrix} \delta R'_{s_X} \\ \delta R'_{s_Y} \\ \delta V'_{s_X} \\ \delta V'_{s_Y} \\ \phi'_{s_X} \\ \phi'_{s_Y} \\ \phi'_{s_Z} \end{bmatrix} , \qquad (69)$$

and not for $\mathbf{x}_S$ or $\mathbf{x}_M$ themselves, whereas the DVS measurements, as defined in Eq.(52) do allow elements of $\mathbf{x}_M$ to be observable. From the viewpoint of observability then, an alternative selection of inertial system error states for the original fully coupled filter could just as well be $\mathbf{x}_M$ and $\mathbf{x}'_s$ instead of $\mathbf{x}_M$ and $\mathbf{x}_S$. In that case, the dynamics of the state vector $\mathbf{x}'_s$ are derived by subtracting Eq.(21) from Eq.(24) to give

$$\dot{\mathbf{x}}'_s = \mathbf{F}_s\mathbf{x}'_s + (\mathbf{F}_{s/IMU}\mathbf{x}_{IMU} - \mathbf{F}_{M/INS}\mathbf{x}_{INS}) + \mathbf{w}'_s \quad , \qquad (70)$$

where

$$\mathbf{w}'_s = \mathbf{w}_s - \mathbf{w}_M \quad , \qquad (71)$$

and it has been assumed that $\mathbf{F}_M \approx \mathbf{F}_s$. This assumption is valid as long as the axes of the master INS and strapdown navigator wander azimuth frames are nearly coincident (i.e. $\mathbf{C}^{MW}_{SW} \approx \mathbf{I}$, the identity matrix) and the relative motion between the master INS and strapdown IMU is small compared to the nominal values of velocity and specific force appearing in the F matrices. Both these conditions are true in this case.

The measurement model for the master INS/strapdown velocity matching measurements is obtained in terms of $\mathbf{x}'_s$ by first writing out the following expression, using Eqs.(56), (57) and (58):

$$\begin{bmatrix} z_{V_X} \\ z_{V_Y} \end{bmatrix} = \mathbf{H}_{V_M}\mathbf{x}_M + \mathbf{H}_{V_s}\mathbf{x}_s \quad , \qquad (72)$$

where $\mathbf{H}_{V_M}$ and $\mathbf{H}_{V_s}$ are given by Eqs.(62) and (63). Substituting $\mathbf{x}_s = \mathbf{x}'_s + \mathbf{x}_M$ into the equation above and assuming again that $\mathbf{C}^{MW}_{SW} \approx \mathbf{I}$ yields

$$\begin{bmatrix} z_{V_X} \\ z_{V_Y} \end{bmatrix} = \mathbf{H}_{V_s}\mathbf{x}'_s \quad . \qquad (73)$$

The form of the above equation clearly confirms that only $\mathbf{x}'_s$ is fundamentally observable from the $\mathbf{z}_V$ measurement.

In order for the optimal TOA filter to be decoupled, the estimation of one set of states $\mathbf{x}_1$ must be mathematically decoupled from the estimation of the second set $\mathbf{x}_2$, where in this case, it is desired that

$$\mathbf{x}_1 = \begin{bmatrix} \mathbf{x}_M \\ \mathbf{x}_{INS} \\ \mathbf{x}_{DVS} \end{bmatrix} , \qquad \mathbf{x}_2 = \begin{bmatrix} \mathbf{x}'_s \\ \mathbf{x}_{IMU} \end{bmatrix} \quad . \qquad (74)$$

For $\mathbf{x}_1$ to be decoupled from $\mathbf{x}_2$, there must be no modelled correlation between $\mathbf{x}_1$ and $\mathbf{x}_2$. In other words, the cross-covariance matrix of $\mathbf{x}_1$ and $\mathbf{x}_2$ must be zero at all times. There are generally three ways that correlation between $\mathbf{x}_1$ and $\mathbf{x}_2$ can be introduced into the Kalman filter:
1) through the measurement model,
2) through the model of the system dynamics,
3) through the initialization of the covariance matrix.

The measurement model for z_{V_X} and z_{V_Y}, as expressed in Eq.(73), is only a function of $\mathbf{x}_2$, and the measurement model for z_{D_X} and z_{D_Y} discussed in Section 3.5 is only a function of $\mathbf{x}_1$. So these measurement models are already in a form that avoids correlation between $\mathbf{x}_1$ and $\mathbf{x}_2$.

Examination of the error dynamics models in Eq.(70) and (21) indicates that correlation will develop between $\mathbf{x}_1$ and $\mathbf{x}_2$ because both $\mathbf{x}_M$ and $\mathbf{x}'_s$ are driven by a common error state term $\mathbf{F}_{INS}\mathbf{x}_{INS}$. However, the error covariance for the states

in $\mathbf{x}_{IMU}$ is modelled as being significantly larger than the error covariance for $\mathbf{x}_{INS}$, so that the effect of $\mathbf{F}_{INS}\mathbf{x}_{INS}$ on the estimation of $\mathbf{x}_s'$ is expected to be much less than the effect of the $\mathbf{F}_{IMU}\mathbf{x}_{IMU}$ term, and can therefore be neglected. There is also a certain amount of correlation between $\mathbf{w}_M$ and $\mathbf{w}_s'$. The cross spectral density matrix for these two process noise vectors, using Eqs.(34) and (42), is found to be

$$\mathbf{Q}'_{M/s} = \mathbf{Q}_{M/s} - \mathbf{Q}_M = \begin{bmatrix} 0 & 0 & 0 & 0 & 0 & 0 & 0 \\ 0 & 0 & 0 & 0 & 0 & 0 & 0 \\ 0 & 0 & -q_{MASF} & 0 & 0 & 0 & 0 \\ 0 & 0 & 0 & -q_{MASF} & 0 & 0 & 0 \\ 0 & 0 & 0 & 0 & -q_{MGN} & 0 & 0 \\ 0 & 0 & 0 & 0 & 0 & -q_{MGN} & 0 \\ 0 & 0 & 0 & 0 & 0 & 0 & -q_{MGN} \end{bmatrix} \quad (75)$$

However, consider the spectral density matrix for $\mathbf{w}_s'$. This matrix $\mathbf{Q}_s'$ is expressed in terms of previously defined spectral density matrices as

$$\mathbf{Q}_s' = \mathbf{Q}_M + \mathbf{Q}_s - 2\mathbf{Q}_{M/s} \quad , \quad (76)$$

which yields

$$\mathbf{Q}_s' = \begin{bmatrix} 0 & 0 & 0 & 0 & 0 & 0 & 0 \\ 0 & 0 & 0 & 0 & 0 & 0 & 0 \\ 0 & 0 & q_{SASF}+q_{MASF} & 0 & 0 & 0 & 0 \\ 0 & 0 & 0 & q_{SASF}+q_{MASF} & 0 & 0 & 0 \\ 0 & 0 & 0 & 0 & q_{SGMU}+q_{MGN} & 0 & 0 \\ 0 & 0 & 0 & 0 & 0 & q_{SGMU}+q_{MGN} & 0 \\ 0 & 0 & 0 & 0 & 0 & 0 & q_{SGMU}+q_{SGSF}+q_{MGN} \end{bmatrix} \quad (77)$$

The principal terms in the above expression that affect the estimation of $\mathbf{x}_s'$ are q_{SGMU} and q_{SGSF}, which, in general, are significantly larger than the q_{MGN} terms that appear in the same locations in the matrix $\mathbf{Q}'_{M/s}$. Consequently, it can be assumed that $\mathbf{Q}'_{M/s} = \mathbf{0}$ with little effect on the estimation of $\mathbf{x}_s'$. It may be noticed that q_{VD} does not appear in Eq.(77). This is consistent with the expectation that vertical deflection errors, which affect both $\mathbf{x}_s$ and $\mathbf{x}_M$ in the same way, should not affect the difference states. Based on the above discussion, the state dynamics models for the two decoupled filters can be written as

$$\begin{aligned} \dot{\mathbf{x}}_1 &= \mathbf{F}_1\mathbf{x}_1 + \mathbf{w}_1 \quad , \\ \dot{\mathbf{x}}_2 &= \mathbf{F}_2\mathbf{x}_2 + \mathbf{w}_2 \quad , \end{aligned} \quad (78)$$

where

$$\mathbf{F}_1 = \begin{bmatrix} \mathbf{F}_M & \mathbf{F}_{M/INS} & \mathbf{0} \\ \mathbf{0} & \mathbf{F}_{INS} & \mathbf{0} \\ \mathbf{0} & \mathbf{0} & \mathbf{F}_{DVS} \end{bmatrix}, \quad \mathbf{w}_1 = \begin{bmatrix} \mathbf{w}_M \\ \mathbf{w}_{INS} \\ \mathbf{w}_{DVS} \end{bmatrix} \quad , \quad (79)$$

and

$$\mathbf{F}_2 = \begin{bmatrix} \mathbf{F}_s & \mathbf{F}_{S/IMU} \\ \mathbf{0} & \mathbf{F}_{IMU} \end{bmatrix}, \quad \mathbf{w}_2 = \begin{bmatrix} \mathbf{w}_s' \\ \mathbf{w}_{IMU} \end{bmatrix} \quad . \quad (80)$$

The initial cross-covariance matrix between $\mathbf{x}_1$ and $\mathbf{x}_2$ is expressed as

$$\mathbf{P}_{12_0} = E[\tilde{\mathbf{x}}_{1_0}\tilde{\mathbf{x}}_{2_0}^T] = \begin{bmatrix} E[\tilde{\mathbf{x}}_{M_0}\tilde{\mathbf{x}}_{S_0}'^T] & E[\tilde{\mathbf{x}}_{M_0}\tilde{\mathbf{x}}_{IMU_0}^T] \\ E[\tilde{\mathbf{x}}_{INS_0}\tilde{\mathbf{x}}_{S_0}'^T] & E[\tilde{\mathbf{x}}_{INS_0}\tilde{\mathbf{x}}_{IMU_0}^T] \\ E[\tilde{\mathbf{x}}_{DVS_0}\tilde{\mathbf{x}}_{S_0}'^T] & E[\tilde{\mathbf{x}}_{DVS_0}\tilde{\mathbf{x}}_{IMU_0}^T] \end{bmatrix} \quad . \quad (81)$$

All of the terms in the above expression are found to be zero except for the initial cross-covariance matrix between $\mathbf{x}_M$ and $\mathbf{x}_s'$. This term is evaluated, with the help of Eqs.(11) and (14), as

$$E[\tilde{\mathbf{x}}_{M_0}\tilde{\mathbf{x}}_{S_0}'^T] = \mathbf{P}_{M/S_0} - \mathbf{P}_{M_0} = \begin{bmatrix} 0 & 0 & 0 & 0 & 0 & 0 & 0 \\ 0 & 0 & 0 & 0 & 0 & 0 & 0 \\ 0 & 0 & 0 & 0 & 0 & 0 & 0 \\ 0 & 0 & 0 & 0 & 0 & 0 & 0 \\ 0 & 0 & 0 & 0 & -\sigma^2_{M\phi} & 0 & 0 \\ 0 & 0 & 0 & 0 & 0 & -\sigma^2_{M\phi} & 0 \\ 0 & 0 & 0 & 0 & 0 & 0 & 0 \end{bmatrix} \quad . \quad (82)$$

The magnitude of the non-zero terms in the above expression is much smaller than the initial variance $\sigma^2_{s\phi}$ assigned to the estimation error for ϕ'_{s_x} and ϕ'_{s_y}. This variance is large to reflect the large uncertainty in the knowledge of the initial roll and pitch of the IMU. Under these conditions then, it can be assumed that $\mathbf{P}_{12_0}=\mathbf{0}$, with little consequence for the estimation of $\mathbf{x}_2$.

In summary then, it can safely be assumed that the three conditions to allow state decoupling, as stated previously in this section, are satisfied for the two vectors $\mathbf{x}_1$ and $\mathbf{x}_2$, and consequently, the optimal TOA filter can be mechanized as two decoupled filters.

It should be noted that for the purposes of closed loop correction of the strapdown navigator parameters, it is still an estimated value of $\mathbf{x}_S$ that is required, not $\mathbf{x}'_S$. Consequently, for this decoupled filter configuration where $\mathbf{x}_S$ is not explicitly estimated, it must be constructed when it is needed as

$$\hat{\mathbf{x}}_S = \hat{\mathbf{x}}_M + \hat{\mathbf{x}}'_S \quad , \tag{83}$$

where the symbol $\hat{}$ denotes estimated quantities.

4.2 State Deletion

If certain error states that are being modelled in the filter are too small to be observable with the given measurement models, then they can often be eliminated with little impact on the filter performance. For example, consider the plots in Figures 9 to 11 obtained from the simulation run with the optimal filter. The solid traces in these plots show the time histories of the master INS gyro bias state estimation errors, and the dashed lines show the filter-computed standard deviations for these estimation errors. It is obvious that the predicted standard deviations do not change significantly from their initial values over the course of the run. This is a clear indication that these states are too small to be observable by the filter.

When states are eliminated, it is usual to attempt to compensate for their loss by adding a component to the process noise. For example, from the expression for $\mathbf{F}_{M/INS}$ in Eq.(27), the first-order effect of a gyro bias state is to cause a linear growth in inertial platform misalignments. Thus, the variance growth for the platform misalignment estimation error as a result of a modelled gyro bias state is given approximately by

$$\sigma^2_{M\phi}(t) = \sigma^2_{MGB}\, t^2 \quad . \tag{84}$$

If the effects of a gyro bias were modelled by a white noise process with spectral density q_{MGB}, then the variance growth for the platform misalignment estimation errors is expressed as

$$\sigma^2_{M\phi}(t) = q_{MGB}\, t \quad . \tag{85}$$

One criterion that the filter designer may use to assign an appropriate value to q_{MGB} is to select a value of q_{MGB} that results in the $\sigma^2_{M\phi}$ buildup being equal for both cases at a chosen time T. This condition is expressed as

$$\sigma^2_{MGB}\, T^2 = q_{MGB}\, T \quad , \tag{86}$$

which yields

$$q_{MGB} = \sigma^2_{MGB}\, T \quad . \tag{87}$$

The choice of T is itself fairly arbitrary, but a suitable choice is the filter settling time, which is in the order of about 1000 seconds. The quantity q_{MGB} computed from the above expression is then added to the q_{MGN} terms in the spectral density matrix $\mathbf{Q}_M$ to compensate for the deletion of the gyro bias states.

Another case for deleting states can be made when it is not important to know the state estimate, and the state does not

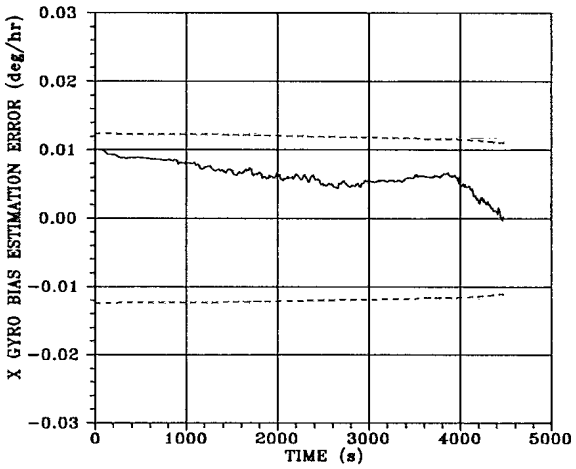

Figure 9. Master INS X Gyro Bias Estimation Error and Predicted Error Standard Deviation (Optimal Filter).

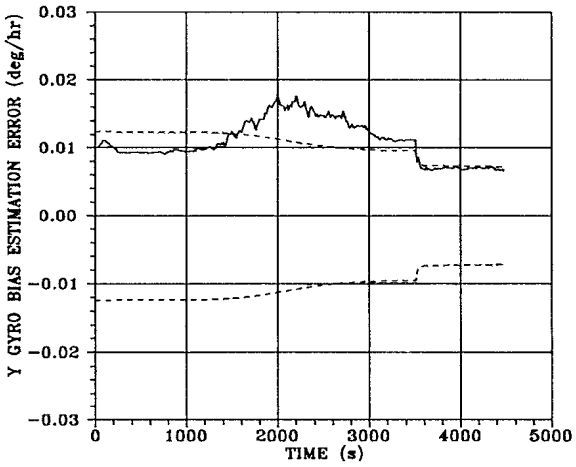

Figure 10. Master INS Y Gyro Bias Estimation Error and Predicted Error Standard Deviation (Optimal Filter).

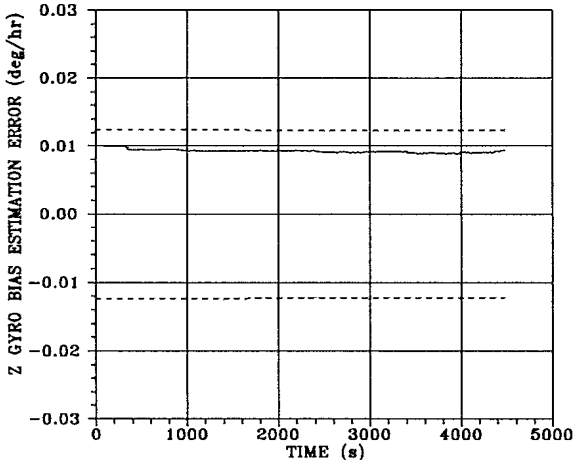

Figure 11. Master INS Z Gyro Bias Estimation Error and Predicted Error Standard Deviation (Optimal Filter).

have a significant effect on the estimation of other states of interest. A good example of this is the position error states modelled for the master INS and the strapdown navigator. The primary requirement for the TOA filter is to control attitude errors and velocity errors in the strapdown navigator. Absolute positional accuracy is not a requirement. Furthermore, deletion of the position error states does not impact on estimation of the other states. This can be seen by considering the measurement model and error dynamics model for the TOA filter. Since the measurement model does not include any terms that contain the position error states, then obviously it is not affected by the absence of these states. With regard to the error dynamics, from examination of the expression for $\mathbf{F}_M$ in Eq.(26), it can be seen that position error terms which drive the velocity errors and platform misalignments are weak compared to other driving terms for these states. The dominant term that would be omitted as a result of deleting the position error states is of the form $\frac{\omega_{IE_Z}}{R}\delta R$. To first order, this term causes a linear growth of platform tilts. Following a similar approach to that taken for the gyro bias states, an appropriate selection for the spectral density of an equivalent white noise process is

$$q_{MR} = \left(\frac{\omega_{IE_Z}}{R}\right)^2 \sigma^2_{MR} T \quad , \tag{88}$$

where σ^2_{MR} is chosen to be the expected variance of the position error over the entire flight, and T, as before, is selected to be the filter settling time. This new spectral density term is included in $\mathbf{Q}_M$ by summing it with the q_{MGN} terms that affect the estimation of platform tilts. A similar spectral density term q_{SR} can be incorporated into $\mathbf{Q}'_s$ to compensate for the deletion of position states from the $\mathbf{x}'_s$ vector.

4.3 Simulation Results

An identical simulation run to that performed for the optimal TOA filter was conducted with the suboptimal filter design. For this run, the modifications to the measurement and error dynamics model discussed in this section were implemented to realize two decoupled filters without position error states or master INS gyro bias states.

The results of the run are shown in Figures 12 to 16 which depict the velocity, attitude and heading estimation errors of the strapdown navigator, along with associated filter-predicted standard deviations, after closed loop correction with the filter-estimated error quantities. From comparison to the corresponding plots in Figures 4 to 8, it is clear that the suboptimal filter performance is very nearly the same as that of the optimal configuration. These results confirm the validity of the model simplifications discussed in this section.

5. CONCLUSIONS

The process of designing a suboptimal *t*ransfer-*o*f-*a*lignment (TOA) Kalman filter for a SAR motion compensation application has been detailed at some length. While a certain amount of the information presented is fairly unique to this particular application, the criteria used in making the filter model simplifications provide useful guidelines for general suboptimal filter design. Also, much of the discussion regarding inertial system behaviour is of course relevant to aerospace navigation applications involving inertial technology. Further information on general principles of suboptimal filter design and implementation can be found in [6].

Specifically, two principal techniques of Kalman filter model simplification, namely state deletion and state decoupling, have been demonstrated for the TOA filter example. Starting with a description of the optimal Kalman filter, the process of designing modifications to accommodate state deletion and decoupling has been discussed, along with the rationale for these modifications. Simulation results for the optimal and suboptimal filter configurations were presented to confirm that the suboptimal filter design provided similar performance to the optimal filter.

6. REFERENCES

1. J.J.Kovaly, *Synthetic Aperture Radar*, Artech House Inc., Dedham, Massachusetts, 1976.

2. M.I.Skolnik, ed., *Radar Handbook*, Chapter 23, McGraw-Hill Book Company, New York, 1970.

3. D.J.DiFilippo, G.E.Haslam, and W.S.Widnall, "Evaluation of a Kalman Filter for SAR Motion Compensation", proceedings of PLANS 88, Orlando, Florida, Nov.29-Dec.2, 1988.

4. R.E.Kalman, "A New Approach to Linear Filtering and Prediction Problems", J. Basic Eng., March 1960, pp.35-46.

5. R.E.Kalman and R.S.Bucy, "New Results in Linear Filtering and Prediction Theory", J. Basic Eng., March 1961, pp.95-108.

6. A.Gelb, ed., *Applied Optimal Estimation*, The M.I.T. Press, Cambridge Massachusetts, 1974.

7. M.Kayton and W.R.Fried, eds., *Avionics Navigation Systems*, Chapter 6, John Wiley and Sons, Inc., New York, 1969.

8. D.O.Benson, "A Comparison of Two Approaches to Pure Inertial and Doppler-Inertial Error Analysis", IEEE Transactions on Aerospace and Electronic Systems, Vol. AES-11, No.4, July 1975, pp.447-455.

9. D.B.Reid and J.Hepburn, "Final Report for SAR Motion Compensation Study", Report H8402-03/SARMC/DBR, Huntec (70) Ltd., February, 1984.

10. G.J.Bierman, *Factorization Methods for Discrete Sequential Estimation*, Academic Press, New York, 1977.

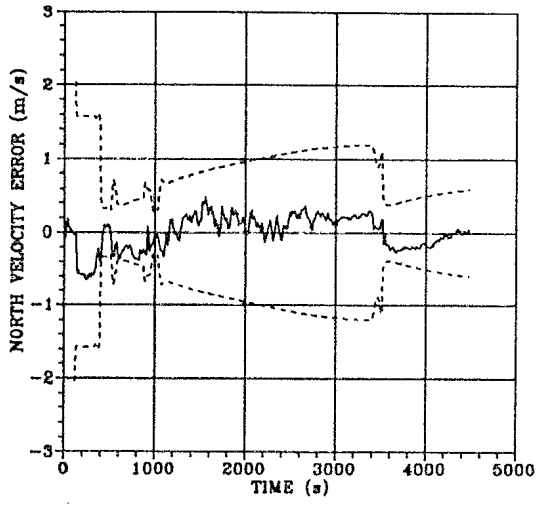

Figure 12. Strapdown Navigator North Velocity Error and Predicted Error Standard Deviation (Suboptimal Filter).

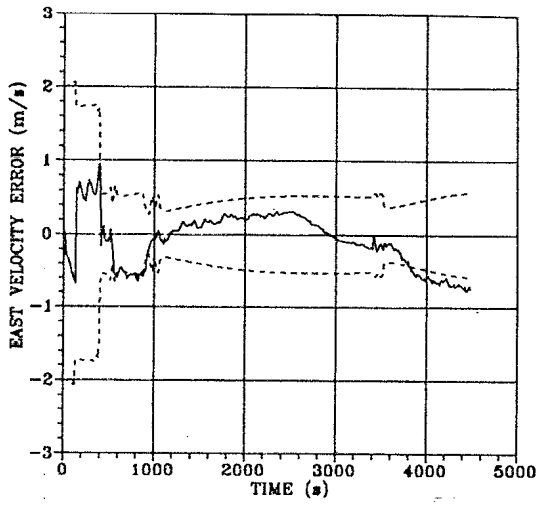

Figure 13. Strapdown Navigator East Velocity Error and Predicted Error Standard Deviation (Suboptimal Filter).

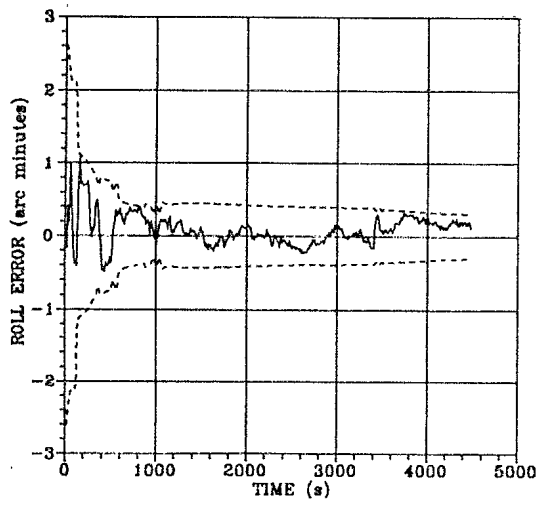

Figure 14. Strapdown Navigator Roll Error and Predicted Error Standard Deviation (Suboptimal Filter).

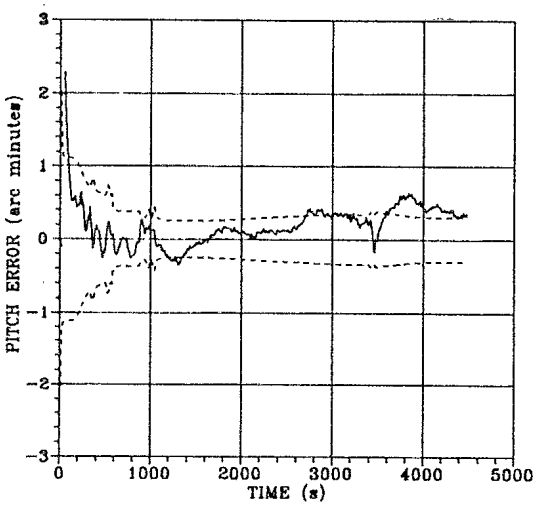

Figure 15. Strapdown Navigator Pitch Error and Predicted Error Standard Deviation (Suboptimal Filter).

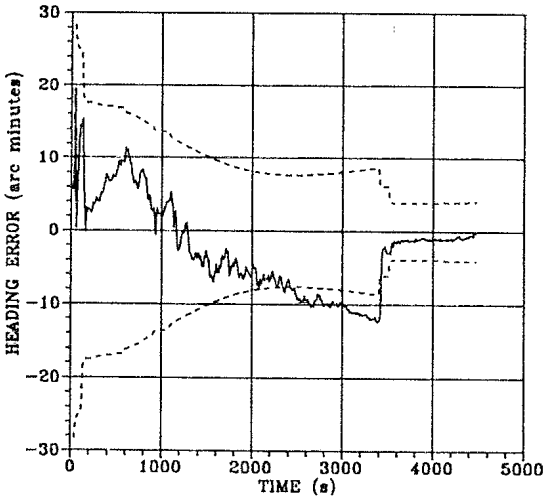

Figure 16. Strapdown Navigator Heading Error and Predicted Error Standard Deviation (Suboptimal Filter).